Hindawi
Journal of Nanomaterials
Volume 2019, Article ID 9170732, 8 pages
https://doi.org/10.1155/2019/9170732

Research Article

Modification of Alginate Hydrogel Films for Delivering Hydrophobic Kaempferol

Yuanfeng Ye,[1,2,3] Xiaojuan Zhang,[1,2] Xiang Deng,[1,2,4] Lingyun Hao,[1,2] and Wei Wang[1,2]

[1]*School of Material Engineering, Jinling Institute of Technology, Nanjing 211169, China*
[2]*Nanjing Key Laboratory of Optometric Materials and Technology, Nanjing 211169, China*
[3]*School of Chemistry and Chemical Engineering, Nanjing University, Nanjing 210023, China*
[4]*College of Materials Science and Engineering, Nanjing Tech University, Nanjing 210000, China*

Correspondence should be addressed to Xiaojuan Zhang; zxj831005@hotmail.com

Received 11 September 2018; Revised 20 November 2018; Accepted 15 December 2018; Published 24 March 2019

Academic Editor: Victor M. Castaño

The high hydrophilicity of alginate materials makes delivering a high load of hydrophobic drug difficult. To overcome this drawback, sodium alginate (SA) was modified using octylamine (OA), and then kaempferol (KP) was combined with the alginate solution through the hydrophobic interaction between OA and KP. The modified SA/KP (MSA/KP) hydrogel films were ionically cross-linked by immersing in calcium chloride solution. Subsequently, the products were analyzed via Fourier transform infrared spectroscopy, scanning electron microscopy, contact angle test, thermogravimetric analysis, swelling analysis, water vapor transmission, and mechanical property test. Results showed that compared with the SA hydrogel films, the MSA/KP hydrogel films exhibited an interporous structure, good swelling, and mechanical properties. Moreover, the drug release experiments demonstrated that the MSA/KP hydrogel films achieved a KP encapsulation efficiency of 70.4%, with a sustained KP release of up to 80 h. The cell viability experiments demonstrated that the MSA/KP hydrogel films posed no evident cytotoxicity to human umbilical vein endothelial cells.

1. Introduction

A hydrogel is a 3D hydrophilic network that can be applied to drug delivery, regenerative medicine, and wound dressing [1]. The use of different materials, such as poly(vinyl alcohol) (PVA), chitosan, alginate, nanofibrillar cellulose, and gelatin, to prepare hydrogels has elicited considerable attention [2–5]. Given its unique biocompatibility, biodegradability, immunogenicity, and nontoxicity [6], alginate has been used as an excellent polysaccharide for preparing hydrogel films. Pereira et al. [7] prepared novel alginate-based hydrogel films via calcium chloride ($CaCl_2$) cross-linking; their films exhibited good swelling ability, transparency, thermal stability, and mechanical properties. Serrano-Aroca et al. [8] developed a series of calcium alginate composite hydrogel films using graphene oxide, which improved water diffusion and mechanical properties. Taira et al. [9] synthesized calcium alginate/gelatin hydrogel films via electrochemical printing; their films demonstrated considerable potential in constructing 3D tissue organs. Su and Chen [10] prepared montmorillonite/alginate/Ca^{2+} nanocomposite hydrogel films through solution casting and subsequent ionic cross-linking; their films presented high transparency, good mechanical properties, and high efficiency in blocking ultraviolet (UV) light.

Alginate-based hydrogel films have also been used in drug delivery systems. Wu et al. [11] prepared chitosan/alginate hydrogel films for delivering lysozyme, which improved antibacterial activity against *Escherichia coli* and *Staphylococcus aureus*. Treenate and Monvisade [12] developed a pH-sensitive chitosan/sodium alginate (SA) hydrogel by using paracetamol as a model drug; they showed that the burst release of paracetamol was depressed by increasing the chitosan content or applying a cross-linker.

Kaempferol (KP), a natural compound, is widely used in antioxidative, anti-inflammatory, antiallergic, and anticancer applications [13, 14]. It has been reported that KP is an effective wound-healing agent in the treatment of both

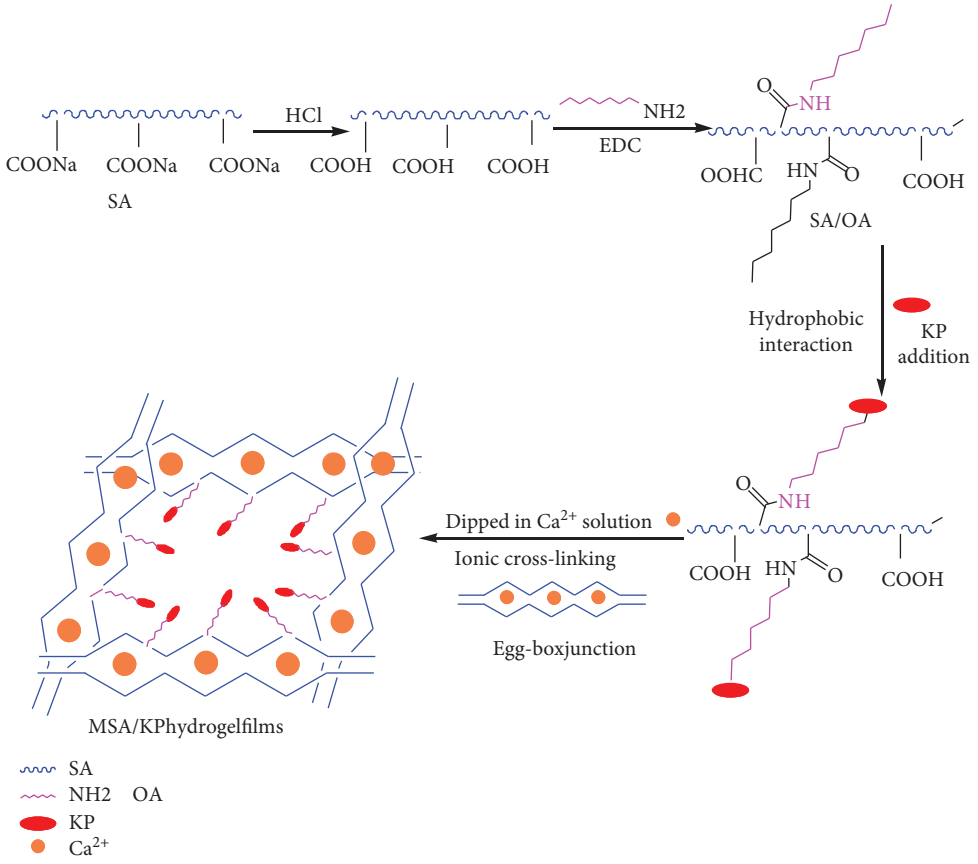

Figure 1: Schematic of the formation of the MSA/KP hydrogel films.

nondiabetic and diabetic wounds [15, 16]. However, its poor water solubility, instability, and short half-life in vivo metabolism limit the clinical applications of KP [17]. To improve its absorption, KP has been loaded into different carriers, such as magnetic microspheres [18], nanoemulsion [19], chitosan nanoparticles [20], phospholipid complex [21], liposome [22], and cyclodextrin [23]. A hydrogel delivery system with a high KP load and a controlled release of KP is worthy of investigation.

In the current study, SA was first modified using octylamine (OA), and then KP was combined with the alginate solution. The modified SA/KP (MSA/KP) hydrogel films were prepared via ionic cross-linking. Furthermore, the properties of the MSA/KP hydrogel films and the biocompatibility of the films with human umbilical vein endothelial cells (HUVECs) were investigated.

2. Experimental

2.1. Materials. SA, 1-ethyl-3-(3-dimethylaminopropyl) carbodiimide (EDC)·hydrochloric acid (HCl), phosphate-buffered saline (PBS), KP, acetone, ethyl alcohol, $CaCl_2$, OA, 3-(4,5-dimethylthiazol-2-yl)-2,5-diphenyltetrazolium bromide (MTT), potassium bromide (KBr), dipotassium phosphate (K_2HPO_4), sodium chloride (NaCl), tris(hydroxymethyl) aminomethane [$(CH_2OH)_3CNH_2$], and hydrochloric acid (HCl) were purchased from Sinopharm Chemical Reagent Co. Ltd. Distilled water from a Milli-Q® water purification system was used.

2.2. Synthesis of the MSA/KP Hydrogel Films. The synthesis of the MSA/KP hydrogel films is shown in Figure 1. First, 0.0047 mol SA was dispersed into 66 mL H_2O, and pH was adjusted to 3.0. Then, 0.0047 mol EDC·HCl was added with continuous stirring at 1000 rpm. When the mixture became homogeneous, 0.0016 mol OA was added to the solution, and the reaction was maintained at 25°C for 24 h. Subsequently, the modified SA was obtained, and 5 mL ethanolic KP solution (1 mg/mL) was added to the modified SA solution. The hydrophobic drug KP could be combined with the modified alginate through the hydrophobic interaction between OA and KP. Afterward, the mixture was cast onto a petri dish and immersed in $CaCl_2$ solution (3 wt.%) for cross-linking. The MSA/KP hydrogel films were obtained and dried at room temperature for 12 h. For comparison, we also synthesized SA hydrogel films without adding EDC, OA, and KP. In addition, MSA hydrogel films were prepared without adding KP.

2.3. Infrared (IR) Spectrum Determination, Scanning Electron Microscopy (SEM), and Contact Angle Test of the Hydrogel Films. A Bruker VECTOR 22 spectrometer was used to measure the IR spectra of the hydrogel films. 50 mg of freeze-dried hydrogel films was milled, mixed with

potassium bromide (KBr), and punched into a pellet to measure the IR spectra. Film morphology was obtained using a scanning electron microscope (model: S-4800). The hydrogel films were cryofractured in liquid nitrogen, and the fractured surfaces were sputter-coated with a thin layer of platinum. The contact angles of the hydrogel films were measured using a contact angle meter (Kruss DSA25, Germany). Millipore water of approximately 10 μL was dropped onto the surface of each hydrogel films, and the contact angle was measured. Each specimen was assayed for five replicates. Thermogravimetric analysis (TGA) was conducted using a thermal analyzer (TA2100, America TA). Samples were heated from 50°C to 600°C at a heating rate of 10°C/min in nitrogen (40 mL/min).

2.4. Swelling Properties of the Hydrogel Films. The swelling rate (SR) was measured in PBS (pH 7.4) at 25°C: (a) SA/KP and (b) MSA/KP hydrogel films. The hydrogel films (2 cm × 2 cm) were dispersed in 100 mL PBS solution at 25°C for 24 h to reach the maximum swelling equilibrium. The SR of the hydrogel films was determined using [24]

$$\mathrm{SR} = \frac{(w_s - w_d)}{w_d} \times 100\%, \quad (1)$$

where w_d is the initial mass of the sample and w_s is the mass of the sample after swelling for 24 h.

2.5. Water Vapor Transmission (WVT) Properties of the Hydrogel Films. The WVT properties of the hydrogel films were measured using the method provided in [25]. A disc-shaped piece of each film was mounted on a vial that contained 5 g dry $CaCl_2{\cdot}2H_2O$ and incubated at 25°C and 84% relative humidity. The assembly was weighed at regular intervals, and weight gain was recorded. WVT was calculated using [26]

$$\mathrm{WVT} = \frac{W}{AT}, \quad (2)$$

where W is the weight gain of the glass vial over 24 h, A is the exposed surface area of the film (m^2), and T represents a day. Thus, WVT is expressed as g/m^2/day.

2.6. Mechanical Properties of the Hydrogel Films. The tensile strength and elongation at break of the SA/KP and MSA/KP hydrogel films were tested using a universal testing machine (Instron, model: 5943) at a crosshead speed of 20 mm/min at room temperature.

2.7. Drug Release of the MSA/KP Hydrogel Films. The drug release efficiency of the MSA/KP hydrogel films was tested in pH 7.4 simulated body fluid (SBF). The SBF was used as the release medium: 1.67 mM K_2HPO_4, 2.5 mM $CaCl_2$, and 137.8 mM NaCl in Milli-Q water were adjusted to pH 7.4 by adding 50 mM of tris(hydroxymethyl) aminomethane [$(CH_2OH)_3CNH_2$] and 1 M hydrochloric acid [27]. Approximately 170 mg of MSA/KP hydrogel films was suspended in a conical flask containing 150 mL SBF, and they were kept in a shaking incubator at 37°C and 95 rpm. The incubated solution (3 mL) was collected and replaced with an equal volume of SBF. KP release was characterized using a UV-visible spectrophotometer (UV1101M054) at 370 nm. The calibration curves were plotted with a serial dilution of known concentrations of KP in SBF. The relationship between the absorbance (Abs) and drug concentration (C) could be described by equation (3). The encapsulation and drug loading efficiencies were calculated using equations (4) and (5), respectively:

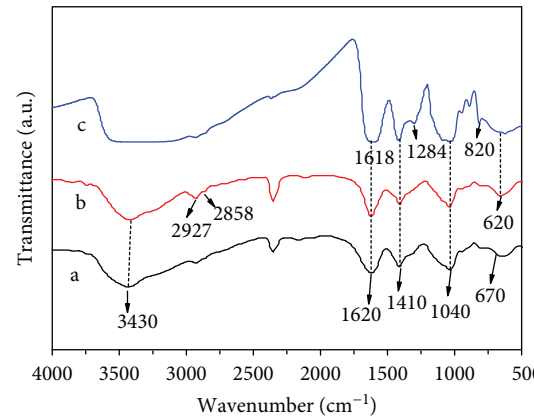

Figure 2: FTIR spectra of the (a) SA, (b) MSA, and (c) MSA/KP hydrogel films.

$$A = 25.096 \cdot C + 0.0003, \quad R^2 = 0.997, \quad (3)$$

$$\text{Encapsulation efficiency} = \frac{m_d}{m_0} \times 100\%, \quad (4)$$

$$\text{Drug loading efficiency} = \frac{m_d}{m_t} \times 100\%, \quad (5)$$

where m_d is the mass of KP in the MSA/KP hydrogel films, m_t is the total mass of the MSA/KP hydrogel films, and m_0 is the total mass of KP.

2.8. In Vitro Cytotoxicity of the MSA/KP Hydrogel Films. HUVECs were selected to measure the cytotoxicity of the MSA/KP hydrogel films by performing the 3-(4,5-dimethylthiazol-2-yl)-2,5-diphenyltetrazolium bromide (MTT) assay [17]. Approximately 200 μL HUVEC was seeded into a 96-well plate. Different concentrations of MSA/KP (0.5, 1, 10, 50, and 100 μg/mL) were added to each group (six wells) for 24 h. Absorbance was measured at a wavelength of 490 nm using a Multiskan FC enzyme-labeled instrument (Thermo Scientific, USA).

3. Results and Discussion

3.1. Fourier Transform IR (FTIR) Analysis. The FTIR spectra of the (a) SA, (b) MSA, and (c) MSA/KP hydrogel films are shown in Figure 2. In Figure 2(a), SA exhibited a broad peak at 3430 cm^{-1} for O–H groups and two peaks at 1620 cm^{-1} and 1410 cm^{-1} for COO^- (asymmetric) and COO^- (symmetric),

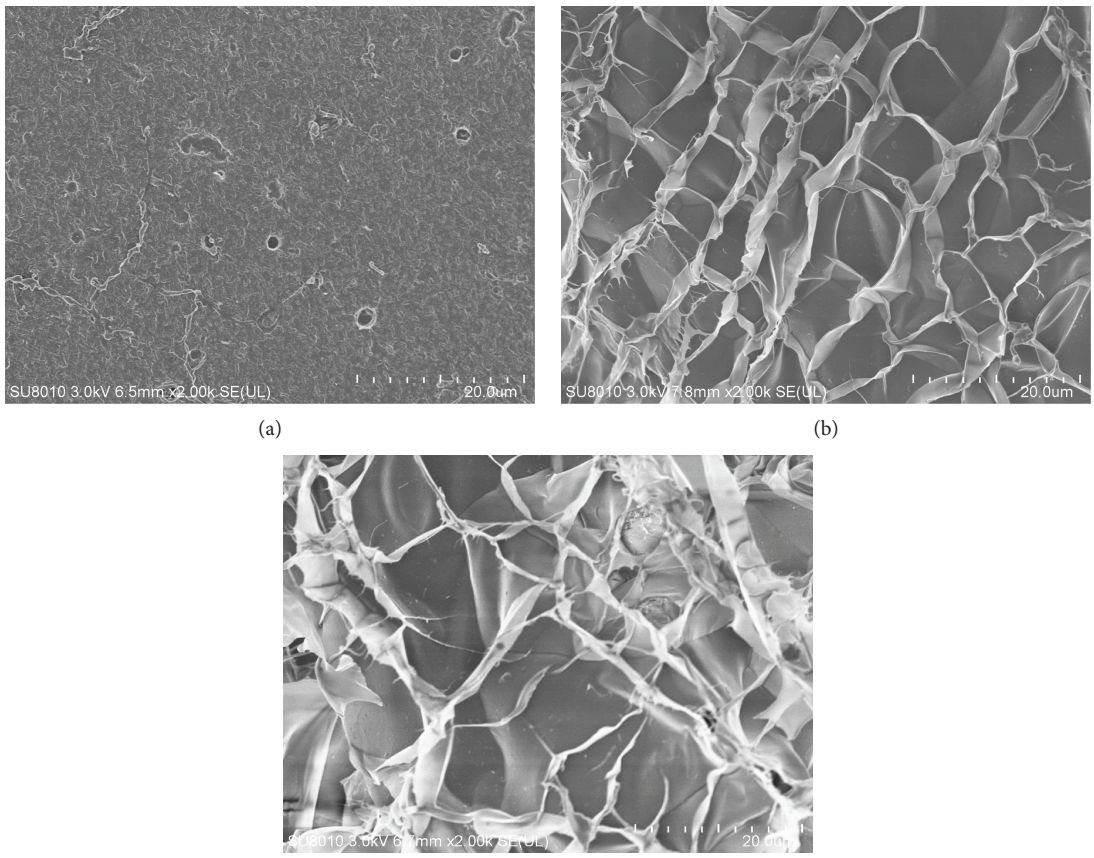

Figure 3: SEM images of the (a) SA, (b) MSA, and (c) MSA/KP hydrogel films.

respectively [28]. The peaks at 820 cm^{-1} and 1040 cm^{-1} could be ascribed to the characteristic peak of the Na–O and C–O bonds, respectively [29]. Moreover, the peak at 670 cm^{-1} corresponded to the vibration of hydroxyl ions. In Figure 2(b), the C=O amide stretching vibration peak appeared at 1620 cm^{-1}. The peaks at 3430, 2927, and 2858 cm^{-1} could be ascribed to the vibration of the –OH, $–CH_3$, and $–CH_2$ bonds, respectively. This result indicated that SA was successfully modified by OA and cross-linked by Ca^{2+} to form a hydrogel. In Figure 2(c), the increased characteristic peaks at 1618 cm^{-1} (C=O stretching in benzene ring) and 1284 cm^{-1} (benzene ring vibrations) could be ascribed to the presence of KP, thereby exhibiting that KP was successfully loaded into the MSA hydrogel films.

3.2. SEM Analysis. The SEM images of the SA, MSA, and MSA/KP hydrogel films are provided in Figure 3. As shown in Figure 3(a), the surface of the SA hydrogel films appears smooth and homogenous with a few irregularly shaped pores, which may be generated by electrostatic repulsions among SA carboxylate anions ($–COO^-$) during polymerization. In Figure 3(b), the surface of the obtained MSA hydrogel films exhibits a 3D porous structure with interconnecting pores after SA modification, which could have improved the loading of the incorporated KP. The morphological structure in Figure 3(c) showed that the drug crystal growth on the surface and the pore size formed decreased. The decrement of the pore size may be attributed to the drug solution entering into the inner side of the sample through these interconnected pores by capillary force [30].

3.3. Contact Angle Analysis. The contact angles of the SA, MSA, and MSA/KP hydrogel films were $45.2^\circ \pm 0.8^\circ$, $111.8^\circ \pm 1.2^\circ$, and $130.7^\circ \pm 1.3^\circ$, respectively. The higher contact angle of the MSA hydrogel films indicated that they were more hydrophobic than the SA hydrogel films because of OA modification [30]. And hydrophobic KP can be successfully loaded into the MSA hydrogel films through the hydrophobic interaction between OA and KP. Accordingly, the contact angle of MSA/KP was higher than the SA and MSA due to the presence of hydrophobic KP.

3.4. TGA. As shown in Figure 4(a), the 36% mass loss before 200°C was due to the desorption of H_2O and the pyrolysis of the oxygen-containing group. The degradation from 200°C to 330°C was attributed to the decomposition of alginate [26]. The pyrolysis of the carbon skeleton was demonstrated by the 12% mass loss between 330°C and 530°C. In Figure 4(b), the 12% weight loss below 215°C was attributed to the loss of H_2O and carboxyl groups. A weight loss of 32% was observed from 215°C to 412°C in Figure 4(b), which was ascribed to the decomposition of SA and OA. A further 19% weight loss between 412°C and 535°C was due to carbon skeleton pyrolysis. In Figure 4(c), the 19% weight loss below

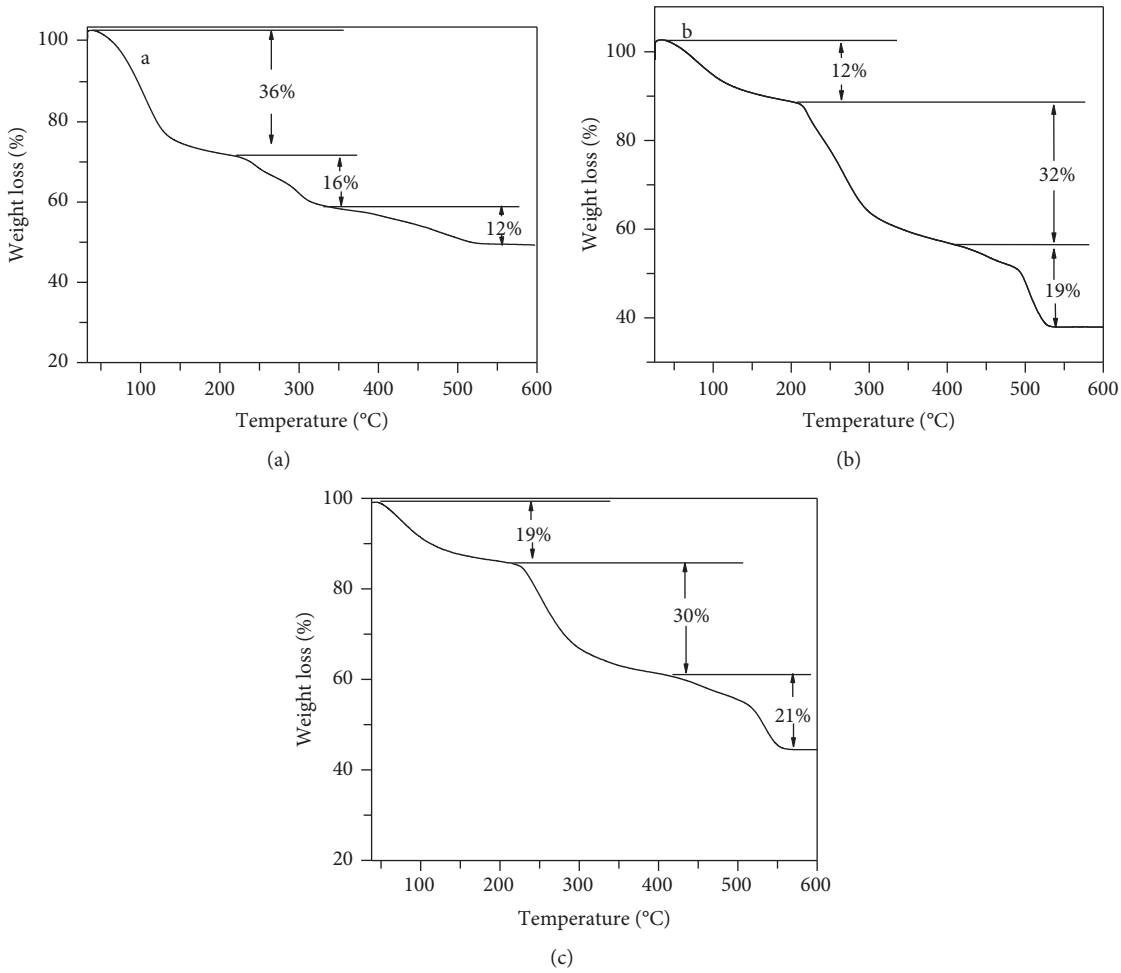

Figure 4: TG curves of the (a) SA, (b) MSA, and (c) MSA/KP hydrogel films.

215°C was attributed to the loss of H_2O and carboxyl groups. A further weight loss of 30% was observed from 215°C to 415°C in Figure 4(c), which was due to the decomposition of SA, OA, and KP. Finally, a 21% weight loss between 415°C and 562°C was ascribed to carbon skeleton pyrolysis.

3.5. Analysis of Swelling Properties. Figure 5 shows the SR of the (a) SA and (b) MSA/KP hydrogel films in pH 7.4 PBS solution at 25°C. In Figure 5(a), the equilibrium SR of SA reached 95.6% at 120 min. In Figure 5(b), the MSA hydrogel films reached swelling equilibrium at 200 min and achieved an SR of 445%. The swelling property of the MSA hydrogel films was better than that of SA hydrogel films, which can be attributed to OA modification. The side chain of OA increased the cross-links and the osmotic pressure of swelling. Meanwhile, the hydrophilic portion was likely to combine with water because the side chain of OA increased the steric hindrance of intramolecular rotation. In Figure 5(c), the MSA/KP hydrogel films reached swelling equilibrium at 200 min and achieved an SR of 344%. The hydrophobic interactions between MSA and KP may tend to reduce chain expansion inside the network, and the swelling of the MSA/KP was depressed [4].

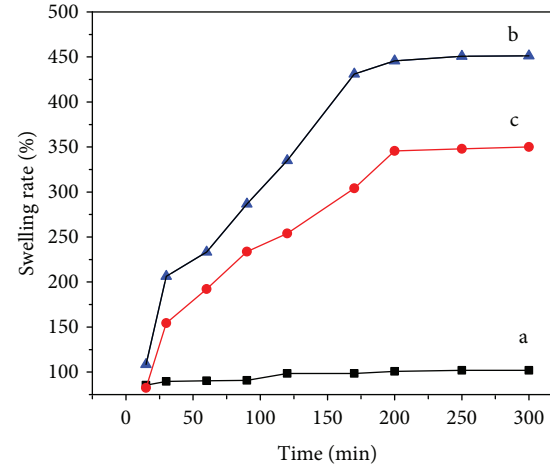

Figure 5: SR of the (a) SA, (b) MSA, and (c) MSA/KP hydrogel films in pH 7.4 solution at 25°C.

3.6. Analysis of WVT Properties. Adequate moisture transmission is crucial for a wound dressing to achieve effective moisture and gas exchange. WVT is essential for evaluating

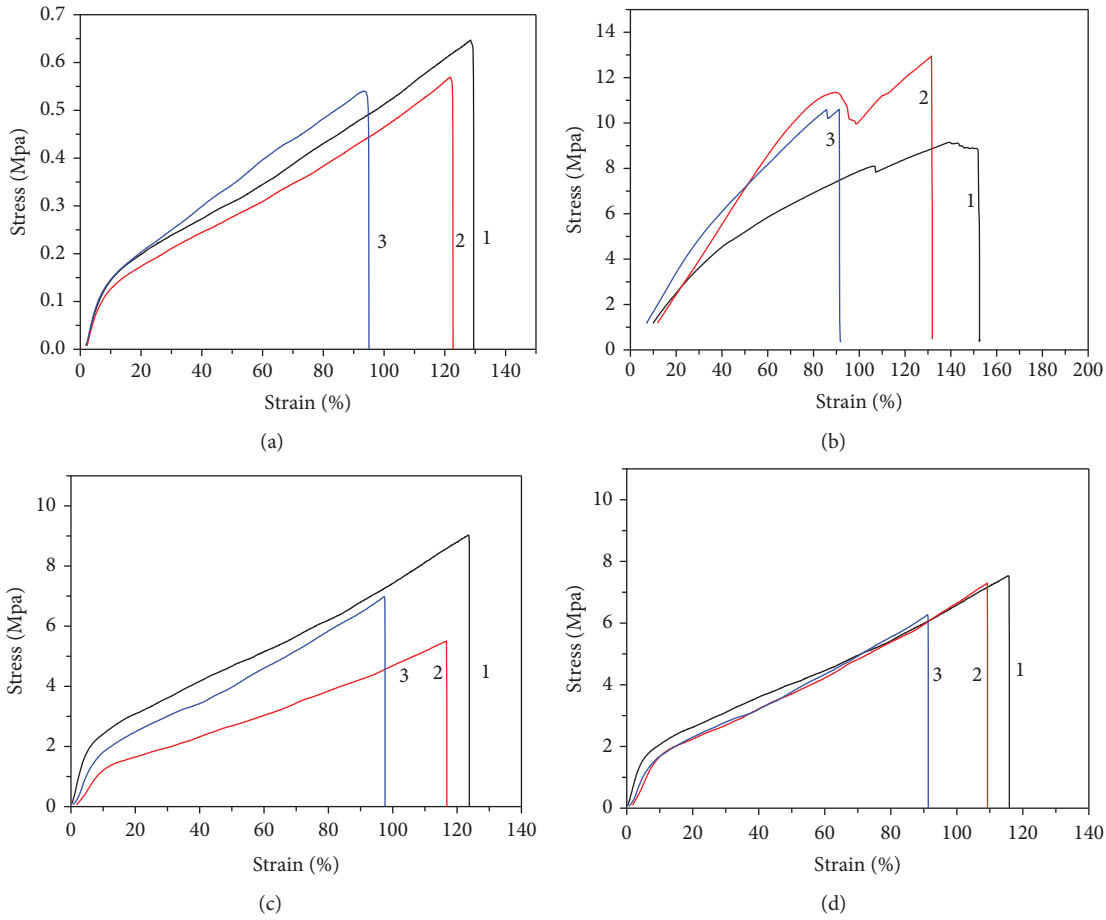

Figure 6: Typical tensile stress-strain curves of the (a) SA, (b) MSA, and (c) MSA/KP hydrogel films and (d) MSA/KP hydrogel films after soaking in 150 mL SBF for 96 h.

hydrogel films as wound dressing [31]. The WVT rates of the SA, MSA, and MSA/KP hydrogel films were 1468.8 g/m^2/day, 6566.4 g/m^2/day, and 5875.2 g/m^2/day, respectively. The WVT rate of an ideal wound dressing should be within 2000–2500 g/m^2/day [26]. Therefore, the MSA/KP hydrogel films are ideal for effective wound healing compared with the SA hydrogel films.

3.7. Analysis of Mechanical Properties. The mechanical properties of the SA and MSA/KP hydrogel films are presented in Figure 6. As shown in Figure 6(a), the tensile strength and elongation at break of the SA hydrogel films were 0.58 MPa and 115.15%, respectively. As shown in Figure 6(b), the MSA hydrogel films exhibited a higher tensile strength (10.76 MPa) and elongation at break (125.3%) than those of the SA hydrogel films. It can be concluded that the addition of OA increased the cross-linking of hydrogel films which provided the higher mobility of the hydrogel matrix. After adding KP, the MSA/KP hydrogel films in Figure 6(c) exhibited lower tensile strength (7.12 MPa) and elongation at break (112.83%) than the MSA hydrogel films. It was due to the fact that the addition of KP into the polymeric network could leave space for the rearrangement of molecular chains in composite films. From Figure 6(d), after soaking in 150 mL SBF for 4 days, the tensile strength and elongation at break of MSA/KP hydrogel films were 6.99 MPa and 105.2%, respectively, which exhibited that the film was still intact and remained strong after 96 h.

3.8. UV Analysis. The release profiles of KP from MSA/KP are shown in Figure 7. The drug loading and encapsulation efficiencies of MSA/KP were 10.3% and 70.4%, respectively.

In Figure 7, the MSA/KP hydrogel films exhibited a severe burst release, and more than 49% KP was released during the first 8 h, which could be attributed to the attachment of the drug on the surface of the hydrogel films. Hence, the rapid release of KP in the first 8 h was probably due to the low molecular weight of KP, which facilitated easy diffusion from the cross-linked hydrogel film network into the medium. The percentage of KP accumulative release from MSA/KP was approximately 58.4%, 48.7%, and 48.4% at 96 h, as shown in Figures 7(a)–7(c), respectively. The slow release phase of KP (12–48 h) may have resulted from the strong hydrophobic interaction between KP and OA.

3.9. In Vitro Cytotoxicity Assay. Cell viability data (Figure 8) indicated that the MSA/KP hydrogel films posed no

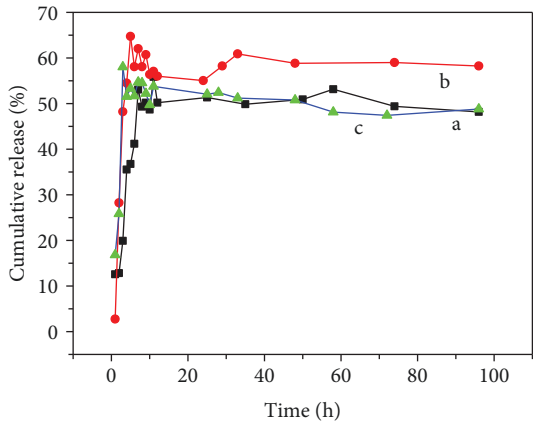

Figure 7: Release behavior of KP from MSA/KP at pH 7.4 SBF: (a), (b), and (c) present the three groups of parallel experiments.

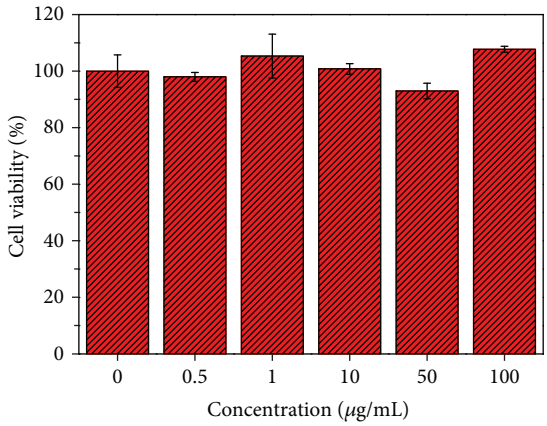

Figure 8: Histogram of cell viability as a function of MSA/KP concentration in the culture media.

considerable cytotoxicity to HUVECs. Different concentrations of the MSA/KP hydrogel films achieved approximately 100% viability after 24 h of incubation. Hence, the MSA/KP hydrogel films demonstrated good biocompatibility with HUVECs, which indicated their suitability for wound healing.

4. Conclusions

KP was successfully introduced into SA hydrogel films via SA modification and subsequent ionic cross-linking. The properties of the MSA/KP hydrogel films were investigated. The SEM images showed that the MSA/KP hydrogel films had a 3D porous structure with interconnecting pores. Compared with the SA hydrogel films, the MSA/KP hydrogel films achieved better swelling, WVT, and mechanical properties. Therefore, the MSA/KP hydrogel films exhibit promising application potential in the wound dressing.

Data Availability

The data used to support the findings of this study are available from the corresponding author upon request.

Conflicts of Interest

The authors declare that they have no conflict of interest.

Acknowledgments

This work was supported by the research grants from Six Talent Peaks Project in Jiangsu Province (no. XCL-109), the sponsorship of the incentive projects of Jinling Institute of Technology (no. Jit-fhxm-201806), the Science and Technology Innovation Project for Overseas Students in Nanjing, the sponsorship of Nanjing Key Laboratory of Optometric Materials and Technology, and the Jiangsu Key Laboratory of Advanced Structural Materials and Application Technology Fund (construction and photocatalytic properties of multifunctional composite porous materials).

References

[1] L. Gritsch, F. L. Motta, N. C. Negrini, L. Yahia, and S. Farè, "Crosslinked gelatin hydrogels as carriers for controlled heparin release," *Materials Letters*, vol. 228, pp. 375–378, 2018.

[2] M. C. G. Pellá, M. K. Lima-Tenório, E. T. Tenório-Neto, M. R. Guilherme, E. C. Muniz, and A. F. Rubira, "Chitosan-based hydrogels: from preparation to biomedical applications," *Carbohydrate Polymers*, vol. 196, pp. 233–245, 2018.

[3] Y. Zhou, C. Zhang, K. Liang et al., "Photopolymerized water-soluble maleilated chitosan/methacrylated poly (vinyl alcohol) hydrogels as potential tissue engineering scaffolds," *International Journal of Biological Macromolecules*, vol. 106, pp. 227–233, 2018.

[4] Y. Wang, W. Wang, X. Shi, and A. Wang, "Enhanced swelling and responsive properties of an alginate-based superabsorbent hydrogel by sodium p-styrenesulfonate and attapulgite nanorods," *Polymer Bulletin*, vol. 70, no. 4, pp. 1181–1193, 2013.

[5] H. Paukkonen, M. Kunnari, P. Laurén et al., "Nanofibrillar cellulose hydrogels and reconstructed hydrogels as matrices for controlled drug release," *International Journal of Pharmaceutics*, vol. 532, no. 1, pp. 269–280, 2017.

[6] Z. Emami, M. Ehsani, M. Zandi, and R. Foudazi, "Controlling alginate oxidation conditions for making alginate-gelatin hydrogels," *Carbohydrate Polymers*, vol. 198, pp. 509–517, 2018.

[7] R. Pereira, A. Carvalho, D. C. Vaz, M. H. Gil, A. Mendes, and P. Bártolo, "Development of novel alginate based hydrogel films for wound healing applications," *International Journal of Biological Macromolecules*, vol. 52, pp. 221–230, 2013.

[8] Á. Serrano-Aroca, J. F. Ruiz-Pividal, and M. Llorens-Gámez, "Enhancement of water diffusion and compression performance of crosslinked alginate films with a minuscule amount of graphene oxide," *Scientific Reports*, vol. 7, no. 1, article 11684, 2017.

[9] N. Taira, K. Ino, J. Robert, and H. Shiku, "Electrochemical printing of calcium alginate/gelatin hydrogel," *Electrochimica Acta*, vol. 281, pp. 429–436, 2018.

[10] X. Su and B. Chen, "Transparent, UV-proof and mechanically strong montmorillonite/alginate/Ca^{2+} nanocomposite hydrogel films with solvent sensitivity," *Applied Clay Science*, vol. 165, pp. 223–233, 2018.

[11] T. Wu, J. Huang, Y. Jiang et al., "Formation of hydrogels based on chitosan/alginate for the delivery of lysozyme and their antibacterial activity," *Food Chemistry*, vol. 240, pp. 361–369, 2018.

[12] P. Treenate and P. Monvisade, "In vitro drug release profiles of pH-sensitive hydroxyethylacryl chitosan/sodium alginate hydrogels using paracetamol as a soluble model drug," *Macromolecules*, vol. 99, pp. 71–78, 2017.

[13] G. Marfe, M. Tafani, M. Indelicato et al., "Kaempferol induces apoptosis in two different cell lines via Akt inactivation, Bax and SIRT3 activation, and mitochondrial dysfunction," *Journal of Cellular Biochemistry*, vol. 106, no. 4, pp. 643–650, 2009.

[14] R. Singh, B. Singh, S. Singh, N. Kumar, S. Kumar, and S. Arora, "Anti-free radical activities of kaempferol isolated from *Acacia nilotica* (L.) Willd. Ex. Del.," *Toxicology In Vitro*, vol. 22, no. 8, pp. 1965–1970, 2008.

[15] Y. Özay, S. Güzel, Ö. Yumrutaş et al., "Wound healing effect of kaempferol in diabetic and nondiabetic rats," *Journal of Surgical Research*, vol. 233, pp. 284–296, 2019.

[16] P. K. Ghosh and A. Gaba, "Phyto-extracts in wound healing," *Journal of Pharmacy & Pharmaceutical Sciences*, vol. 16, no. 5, pp. 760–820, 2013.

[17] X. Zhang, Q. Pan, L. Hao et al., "Preparation of magnetic fluorescent dual-drug nanocomposites for codelivery of kaempferol and paclitaxel," *Journal of Wuhan University of Technology-Materials Science Edition*, vol. 33, no. 1, pp. 256–262, 2018.

[18] X. Zhang, M. Xu, Z. Zhang et al., "Preparation and characterization of magnetic fluorescent microspheres for delivery of kaempferol," *Materials Technology*, vol. 32, no. 3, pp. 125–130, 2017.

[19] M. Colombo, F. Figueiró, A. de Fraga Dias, H. F. Teixeira, A. M. O. Battastini, and L. S. Koester, "Kaempferol-loaded mucoadhesive nanoemulsion for intranasal administration reduces glioma growth in vitro," *International Journal of Pharmaceutics*, vol. 543, no. 1-2, pp. 214–223, 2018.

[20] S. Ilk, N. Sağlam, M. Özgen, and F. Korkusuz, "Chitosan nanoparticles enhances the anti-quorum sensing activity of kaempferol," *International Journal of Biological Macromolecules*, vol. 94, Part A, pp. 653–662, 2017.

[21] K. Zhang, L. Gu, J. Chen et al., "Preparation and evaluation of kaempferol–phospholipid complex for pharmacokinetics and bioavailability in SD rats," *Journal of Pharmaceutical and Biomedical Analysis*, vol. 114, pp. 168–175, 2015.

[22] M. Huang, E. Su, F. Zheng, and C. Tan, "Encapsulation of flavonoids in liposomal delivery systems: the case of quercetin, kaempferol and luteolin," *Food & Function*, vol. 8, no. 9, pp. 3198–3208, 2017.

[23] C. Jullian, V. Brossard, I. Gonzalez, M. Alfaro, and C. Olea-Azar, "Cyclodextrins-kaempferol inclusion complexes: spectroscopic and reactivity studies," *Journal of Solution Chemistry*, vol. 40, no. 4, pp. 727–739, 2011.

[24] T. K. Giri, D. Thakur, A. Alexander et al., "Biodegradable IPN hydrogel beads of pectin and grafted alginate for controlled delivery of diclofenac sodium," *Journal of Materials Science: Materials in Medicine*, vol. 24, no. 5, pp. 1179–1190, 2013.

[25] M. Rezvanian, C.-K. Tan, and S. F. Ng, "Simvastatin-loaded lyophilized wafers as a potential dressing for chronic wounds," *Drug Development and Industrial Pharmacy*, vol. 42, no. 12, pp. 2055–2062, 2016.

[26] M. Rezvanian, N. Ahmad, M. C. I. Mohd Amin, and S. F. Ng, "Optimization, characterization, and in vitro assessment of alginate-pectin ionic cross-linked hydrogel film for wound dressing applications," *International Journal of Biological Macromolecules*, vol. 97, pp. 131–140, 2017.

[27] P. Peng, N. H. Voelcker, S. Kumar, and H. J. Griesser, "Concurrent elution of calcium phosphate and macromolecules from alginate/chitosan hydrogel coatings," *Biointerphases*, vol. 3, no. 4, pp. 105–116, 2008.

[28] S. F. Mohamed, G. A. Mahmoud, and M. F. A. Taleb, "Synthesis and characterization of poly(acrylic acid)-*g*-sodium alginate hydrogel initiated by gamma irradiation for controlled release of chlortetracycline HCl," *Monatshefte für Chemie - Chemical Monthly*, vol. 144, no. 2, pp. 129–137, 2013.

[29] M. F. Abou Taleb, A. Alkahtani, and S. K. Mohamed, "Radiation synthesis and characterization of sodium alginate/chitosan/hydroxyapatite nanocomposite hydrogels: a drug delivery system for liver cancer," *Polymer Bulletin*, vol. 72, no. 4, pp. 725–742, 2015.

[30] T. W. Chung, T. H. Chou, and K. Y. Wu, "Gelatin/PLGA hydrogel films and their delivery of hydrophobic drugs," *Journal of the Taiwan Institute of Chemical Engineers*, vol. 60, pp. 8–14, 2016.

[31] J. J. Elsner and M. Zilberman, "Novel antibiotic-eluting wound dressings: an in vitro study and engineering aspects in the dressing's design," *Journal of Tissue Viability*, vol. 19, no. 2, pp. 54–66, 2010.